Am J Transl Res 2018;10(2):334-351
www.ajtr.org /ISSN:1943-8141/AJTR0068132

*Original Article*

# High-voltage pulsed electric field plus photodynamic therapy kills breast cancer cells by triggering apoptosis

Haixia Zhang[1], Kuangpeng Liu[1], Zhixiao Xue[1], Huijuan Yin[2], Huajiang Dong[2], Wendong Jin[2], Xiafei Shi[2], Han Wang[2], Hai Wang[2]

*[1]Biomedical Engineering and Technology College, Tianjin Medical University, Tianjin 300070, China; [2]Lab of Laser Medicine, Institute of Medical Engineering, Chinese Academy of Medical Sciences and Peking Union Medical College, Tianjin 300192, China*

Received June 27, 2017; Accepted December 25, 2017; Epub February 15, 2018; Published February 28, 2018

**Abstract:** This study evaluated the effects and mechanism of action of combining irreversible electroporation (IRE) and photodynamic therapy (PDT) in breast cancer cells *in vitro* and *in vivo*. Jin's formula was used to assess killing efficacy of different IRE+PDT dosing combinations in breast cancer MCF-7 cells. Flow cytometry, high-content imaging, and confocal laser scanning microscopy were used to detect apoptosis. qRT-PCR and western blotting were used to evaluate expression of apoptosis-related genes and proteins. IRE+PDT combination therapy was administered to BALB/C mice with breast cancer tumors in vivo; tumor size was used to assess treatment efficacy. Killing mechanisms were examined using transmission electron microscopy and immunohistochemistry. We found that IRE+PDT combination therapy produced significant synergistic killing effects in breast cancer cells (highest Jin q value of 1.32). Early apoptosis rates were significantly higher in the IRE+PDT group (16.0%) than in IRE-alone (7.6%) and PDT-alone (4.6%) groups ($P<0.05$). qRT-PCR showed higher Caspase-1, -3, -5, -6, -7, -8, and -9 and TNFRSF1A expression with IRE+PDT than with control. Western blots showed increased cleaved Caspase-3, -7, and -9, and PARP levels in the IRE+PDT group. *In vivo* tumor suppression rate for IRE (1200 V)+PDT (10 mg/kg) was 68.3%. Combination therapy produced the most obvious apoptosis effects. Compared with controls, the IRE+PDT group exhibited lower new blood vessel (VEGF, CD31), metastasis (TGF-β), and cell proliferation (Ki-67) indicators and higher inflammation indicator (TNF-α) 1 day post-treatment. Thus, combining IRE and PDT enhanced their anti-tumor effects in breast cancer, and apoptosis played a key role in this process.

**Keywords:** High-voltage pulsed electric field, photodynamic therapy, breast cancer, combination therapy, apoptosis

## Introduction

Breast cancer is one of the most common malignancies in women around the world. According to the International Agency for Research on Cancer statistics, the global number of new cases of breast cancer in women reached 1.38 million in 2008, accounting for 23% of all female malignancies. Approximately 46 million women died from breast cancer, accounting for 14% of all female cancer deaths [1]. Breast cancer is a serious threat to women's physical and mental health.

Electroporation is a process whereby cells are exposed to short pulses of a high-voltage electric field, increasing the permeability of cell membranes for ions and molecules and forming nanometer-sized fissures. Under certain conditions (e.g., strong electric fields), this increased permeability is permanent, termed irreversible electroporation (IRE). In 2005, Davalos et al. [2] reported that IRE is an ablation method that can avoid thermal tissue damage. In 2006, Edd et al. [3] demonstrated IRE-mediated tissue ablation in normal Sprague-Dawley rat livers, documenting cell death and immunological reactivity in the ablation area. Since then, many researchers have used healthy organs [4, 5] and tumor models [6, 7] of small and large animals to demonstrate that IRE can ablate tumor tissue in a non-thermal manner. After positive results in animal experiments, clinical investigations of IRE began; IRE

has been investigated for the treatment of liver [8, 9], pancreatic [10, 11], kidney [12, 13], lung [14, 15], and prostatic [16] cancers. As a non-thermal, minimally invasive ablation technology, IRE allows tissue selectivity, preserving key structures [17] such as large vessels and nerves in the ablation area, avoiding heat sink effects [18], reducing inflammation [19] and scar formation after treatment, shortening treatment cycles, and enabling real-time monitoring. IRE ablation has many advantages over current ablation technologies.

Despite the potential effectiveness of IRE for treating solid tumors, there are problems that require resolution. IRE-dependent ablation requires distribution of the electric field and conductivity in the target tissue [20]. The former is governed by the configuration of electrodes, and the latter is subject to microenvironmental changes within tissues, cell types, and cellular structures within tissues [21]. Currently, electrode configuration in IRE treatment is designed with a software simulation according to tumor images, but the tumor boundary conditions used in the software simulation are optimized with uniform electric field distribution, which differs from the complex structure, multiple parameters, and versatile surroundings of real tissue. In 2009, Daniels et al. [22] reported that tissue heterogeneity significantly affected the distribution of electric fields and temperatures, and simulation software cannot accurately provide tissue targeting characteristics. The residual tumor boundary in IRE ablation affects cure rates [23] and can lead to recurrence [15]. When using IRE, it is common to see overtreatment or undertreatment, so relying solely on IRE has clear shortcomings. Furthermore, although various ablation technologies have been combined with other treatment methods, such as surgery, chemotherapy, and radiotherapy, the merits of combined therapy are controversial, as these therapies also have side effects.

Photodynamic therapy (PDT) is a relatively new tumor treatment method. It uses lasers of particular wavelengths to illuminate and activate a photosensitizer taken up by tumor tissues, causing a photochemical reaction to produce substances, such as singlet oxygen, that damage tumor cells. PDT has advantages, including dual targeting of the photosensitizer and illumination area, the ability to be used in repeated treatments, long-term immunological effects, and only minimal side effects (e.g., skin allergic reaction). These have allowed PDT to be rapidly developed and extensively used in clinical applications. The United States Food and Drug Administration has already approved PDT for a variety of solid tumors, including tongue, laryngeal, and skin cancers.

In theory, the controllable illumination area of PDT can compensate for the incomplete ablation boundary with IRE, and the electroporation of cell membranes can improve cellular ingestion of the photosensitizer. Therefore, the objective of this research was to evaluate the effects of combining IRE and PDT on breast cancer cells *in vitro* and *in vivo* by evaluating cell toxicity and determining Jin's formula. We also explored the mechanism of action of the combination. Our results show that IRE+PDT combination therapy is more effective than either therapy alone, and may resolve the problem of residual tumor boundary that can occur with IRE ablation alone.

## Materials and methods

### *Materials*

Both the human breast cancer cell line MCF-7 and murine breast cancer cell line EMT-6 were purchased from the cell resource center of the Institute of Basic Medical Sciences, Chinese Academy of Medical Sciences (http://www.cellresource.cn/). BALB/C mice were purchased from Beijing Vital River Laboratory Animal Technology Co., Ltd. Hyclone Roswell Park Memorial Institute (RPMI) 1640 (SH30027.01) culture medium and Gibco fetal bovine serum (FBS; 16000-044) were obtained from Thermo Fisher Scientific (Waltham, MA, USA). Photocarcinorin (PSD-007, 10 mg/mL) was purchased from Zhangjiang Biotechnology Co., Ltd. (Shanghai, China), and phosphate buffer and thiazolyl blue (MTT) were obtained from Sigma (USA). Hoechst 33342 staining solution, Annexin V-Alexa Fluor 488/PI (C1063) apoptosis detection kit, and sodium dodecyl sulfate polyacrylamide gel electrophoresis (SDS-PAGE) rapid preparation kits were purchased from Beyotime Biotechnology Co., Ltd. (Shanghai, China). miRNA Purification Kit (CW06275) and miRNA cDNA Synthesis Kit (CW21415) were purchased from ComWin Biotech Co., Ltd. (Beijing, China). Fast Super EvaGreen qPCR Master mix (s-2008) was purchased from Suzhou Yuheng Biological Technology Co., Ltd. Quantitative reverse tran-

scription-polymerase chain reaction (qRT-PCR) primers were designed in-house and synthesized by Invitrogen (Carlsbad, CA, USA). Apoptosis antibody detection kit (9915) was purchased from Cell Signaling Technology (USA). EasySee Western Blot Kit was purchased from Beijing TransGen Biotech Co., Ltd. (Beijing, China). The ECM830 electroporation apparatus was made by Harvard Apparatus (USA), and the 635-nm semiconductor laser unit was produced by the Institute of Biomedical Engineering, Chinese Academy of Medical Sciences.

*Cell culture*

MCF-7 and EMT-6 cells were cultured at 37°C in a 5% $CO_2$ incubator with RPMI 1640 (Hyclone) containing 10% inactivated FBS, 100 μg/mL penicillin, and 100 μg/mL streptomycin (Gibco). Cells were passaged once every 2-3 days, and cells in the logarithmic growth phase were used for experimentation.

*Cell-based protocols*

*Irreversible electroporation:* An ECM830 square wave generator was used to conduct IRE. MCF-7 cells growing in the logarithmic phase were collected, digested with trypsin, and centrifuged for 5 min. The concentration of the cell suspension was then adjusted to $8 \times 10^4$ cells/mL. Subsequently, 600 μL of cell suspension was added to the electric pulse cup with 4-mm electrode spacing, and pulsed electric fields with 50 pulses were used to pulse the cells at 0, 280, 320, 360, 400, 440, 480, 520, 560, 600, or 640 V, with a pulse length of 100 μs and pulse interval of 1 s. After pulsing, cells were transferred into a 96-well plate and incubated for 24 h. MTT (5 mg/mL) was then added to the culture for 4 h, followed by the addition of dimethyl sulfoxide for 15 min. A microplate reader was used to detect absorbency at 570 nm. The cell survival rate was calculated, and the IRE dose groups with death rates of 20%, 30%, and 40% were selected for further investigations.

*Photodynamic therapy:* MCF-7 cells ($8 \times 10^4$ cells/mL) growing in the logarithmic phase were inoculated into 96-well plates. After overnight incubation, they were cultured together with the photosensitizer (PSD-007) in darkness for 2 h, at PSD-007 concentrations of 0, 3.125, 6.25, 12.5, 25, and 50 μg/mL. After washing twice with phosphate-buffered saline (PBS), a 635-nm laser unit was used to vertically illuminate the cells for 2 min, with a power density of 20 mW/cm$^2$ and energy density of laser (EDL) of 2.4 J/cm$^2$. The cells were cultured for another 24 h, then the death rate was determined using the above MTT methods. PDT dose groups with death rates of 20% and 40% were selected for further investigations.

*Irreversible electroporation + photodynamic therapy:* All experiments were conducted with the following: a control group; IRE-alone groups A (IRE-A; 180 V), B (IRE-B; 280 V), and C (IRE-C; 380 V), with electrode spacing of 4 mm, pulse length of 100 μs, pulse interval of 1 s, and 50 pulses; PDT-alone group I (PDT-I; 10 μg/mL PSD-007) and II (PDT-II; 12.5 μg/mL PSD-007), with 2.4 J/cm$^2$ EDL; and combination therapy groups. The combination therapy groups included IRE-A+PDT-I, IRE-A+PDT-II, IRE-B+PDT-I, IRE-B+PDT-II, IRE-C+PDT-I, and IRE-C+PDT-II. The cells were cultured with the photosensitizer PSD-007 for 5 min in darkness at room temperature. The combination therapy groups then received the electric pulses, which were followed immediately by illumination. The IRE-alone and PDT-alone groups were processed in a similar manner. The cells were subsequently cultured for another 24 h, and the MTT method was used to detect the cell death rate.

*Assessment of combination therapy:* Jin's formula was used to estimate whether IRE and PDT were synergistic. This formula is as follows: $q=E_{a+b}/(E_a+E_b-E_a \cdot E_b)$, with $E_{a+b}$ representing the inhibition rate of methods a and b, and $E_a$ and $E_b$ representing the inhibition rates of methods a and b alone. A *q* value from 0.85 to 1.15 indicates an additive effect, a *q* value more than 1.15 indicates a synergistic effect, and a *q* value less than 0.85 indicates an antagonistic effect.

*Irreversible electroporation effects on the emission spectrum and absorption rate of the photosensitizer:* The 50 μg/mL photosensitizer solution was pulsed using the pulsed electric field with 50 pulses at 380 V, pulse length of 100 μs, and pulse interval of 1 s. A fluorescence spectrophotometer was used to measure the emission spectrum of the photosensitizer before and after the electric pulses, with a 405-nm excitation wavelength for PSD-007.

The above dose parameters were used to treat MCF-7 cells, which were cultured for 0, 0.5, 1,

**Table 1.** Primer names and associated sequences

| Primer names | Sequences | Primer names | Sequences |
|---|---|---|---|
| Casp1-human-F | CCTGGTGTGGTGTGGTTTA | Casp10-human-F | GAGGAAGGCAGCTGGTATATT |
| Casp1-human-R | ATCCTTCTCTATGTGGGCTTTC | Casp10-human-R | GACAGCAGTGAGGATGGATAAG |
| Casp2-human-F | TTCTGGAGAAGGACATCATCAC | TNF-human-F | CCAGGGACCTCTCTCTAATCA |
| Casp2-human-R | GTTCCACATTCTGGCTGAAAC | TNF-human-R | TCAGCTTGAGGGTTTGCTA |
| Casp3-human-F | CTCCACAGCACCTGGTTATT | TNFRSF1A-human-F | CTCCAAATGCCGAAAGGAAATG |
| Casp3-human-R | AAATTCAAGCTTGTCGGCATAC | TNFRSF1A-human-R | ATAATGCCGGTACTGGTTCTTC |
| Casp4-human-F | CCCTCAAGCTTTGTCCTCAT | FAS-human-F | GGGAAGGAGTACACAGACAAAG |
| Casp4-human-R | GCGGTTGTTTCTCTCCTTTATTG | FAS -human-R | GGTCCGGGTGCAGTTTAT |
| Casp5-human-F | CATCCTTGGCACTCATCTCTT | FASLG-human-F | TGCAGCAGCCCTTCAATTA |
| Casp5-human-R | TCCTTCTCCTCGTGGATCTT | FASLG-human-R | AGAGGTTGGACAGGGAAGA |
| Casp6-human-F | GCTGACTTCCTCATGTGTTACT | BCL2-human-F | GGAGGATTGTGGCCTTCTTT |
| Casp6-human-R | TCCCAACATCTCACACAAATCT | BCL2-human-R | GTTCAGGTACTCAGTCATCCAC |
| Casp7-human-F | CTGACTTCCTCTTCGCCTATTC | BID-human-F | CCTACCCTAGAGACATGGAGAA |
| Casp7-human-R | CTGACTTCCTCTTCGCCTATTC | BID-human-R | GTGCGTAGGTTCTGGTTAATA |
| Casp8-human-F | GGAGCTGCTCTTCCGAATTA | CYCS-human-F | TTACACAGCCGCCAATAA |
| Casp8-human-R | CATGACCCTGTAGGCAGAAA | CYCS-human-R | CAGGGATGTACTTCTTGGGATTC |
| Casp9-human-F | GAGTCAGGCTCTTCCTTTGT | β-actin-human-F | GGACCTGACTGACTACCTCAT |
| Casp9-human-R | CTTTGCTGCTTGCCTGTTAG | β-actin-human-R | CGTAGCACAGCTTCTCCTTAAT |

2, 3, and 4 h. An InCell Analyzer 2000 (GE Healthcare Life Sciences, Piscataway, NJ, USA) high-content cell imaging analysis system was then used to analyze and calculate fluorescence intensity, with a 405-nm excitation wavelength for PSD-007 and an emission wavelength of 630 nm.

*Apoptosis detection*

*High-content cell analysis:* MCF-7 cells were divided into groups and cultured for 24 h. The groups were as follows: IRE-alone I (630 V) and IRE-alone II (580 V), with pulse length of 100 μs, pulse interval of 1 s, 50 pulses; PDT-alone I (32 μg/mL PSD-007) and PDT-alone II (29.5 μg/mL PSD-007), with 2.4 J/cm$^2$ EDL; and IRE+PDT-I (380 V+12.5 μg/mL) and IRE+PDT-II (380 V+10 μg/mL), with pulse length of 100 μs, pulse interval of 1 s, 50 impulses, and EDL of 2.4 J/cm$^2$. Next, the Annexin V-FITC apoptosis detection kit and Hoechst 33342 were used to stain the cells, which were analyzed using an InCell Analyzer 2000. The excitation wavelengths for Annexin V-Alexa 488, propidium iodide (PI), and Hoechst 33342 were 490/20 nm, 543/22 nm, and 400/50 nm, respectively, with corresponding emission wavelengths of 525/30 nm, 605/64 nm, and 455/50 nm, respectively.

*Flow cytometry:* The three groups with the highest apoptosis levels were selected through the high-content cell imaging analysis system; they were the IRE-alone II, PDT-alone II, and IRE+PDT-II groups. Cells treated with IRE-II, PDT-II, and IRE+PDT-II were then cultured for 0, 2, or 6 h, collected, and stained with the Annexin V-FITC apoptosis detection kit. The apoptosis rate at the excitation wavelength of 488 nm was determined using a flow cytometer C6 (BD Bioscience, San Diego, CA, USA), analyzing 1 × 10$^4$ cells.

*Confocal laser scanning microscopy:* Cells treated with IRE+PDT combination therapy were cultured for 2 h, stained with AnnexinV/PI and Hoechst 33342, and observed with a laser scanning confocal microscope (Zeiss LSM 710). The excitation and emission wavelengths of AnnexinV were 488 nm and 536 nm, respectively. The corresponding wavelengths were 543 nm and 643 nm for PI and 405 nm and 451 nm for Hoechst 33342.

*Detection of apoptosis-related genes and proteins*

*Real-time quantitative reverse transcription-polymerase chain reaction assay:* Cells treated with IRE, PDT, and IRE+PDT were cultured for 2 h. Total RNA was then extracted using the miRNA Purification Kit following the manufacturer's instructions. The extracted RNAs were subjected to SimpliNano (Biochrom, US) for purity and concentration evaluation and con-

verted to cDNA using the miRNA cDNA Synthesis Kit. The cDNA was used as a template to magnify target genes using Fast Super EvaGreen qPCR Master mix on the ABI 7500 real-time PCR amplifier (Thermo Fisher Scientific). The reverse and forward primers for the target genes and housekeeping genes (β-actin) are listed in **Table 1**. Results were obtained using the ΔΔt method. All reactions were performed at a denaturation temperature of 95°C, annealing temperature of 60°C, and extension temperature of 72°C, repeated for 35-40 cycles.

*Western blot analysis of apoptosis-related proteins expression:* Western blot assays were performed as follows. After 6 h of treatment, cells were collected on ice and lysed in radioimmunoprecipitation assay (RIPA) buffer. The lysate was cleared by centrifugation at 12,000 × g for 5 min, then heated at 100°C for 10 min in reducing buffer. Samples (30 μg) were separated by SDS-PAGE and transferred onto polyvinylidene fluoride membranes. After transfer to nitrocellulose, the membrane was incubated in blocking solution (5% skimmed milk and Tris-buffered saline with Tween 20 [TBST]) for 1 h at room temperature. Membranes were then incubated overnight with the primary antibody (1:1000 dilution) at 4°C. The membranes were subsequently washed with TBST, then incubated with the second antibody (1:1000 dilution) for 1 h at room temperature, followed by washing with TBST. We then used the EasySee Western Blot Kit and visualized the protein bands via the Clinx ChemiScope Series Chemiluminescence Imaging systems (Clinx Science, China). β-actin was used as a loading control.

*Animal experimentation*

*Murine breast cancer model:* All animal experiments were approved by the animal care and use committee of the Institute of Medical Engineering, Chinese Academy of Medical Sciences or Biomedical Engineering and Technology College (2015015).

Murine breast cancer cells (EMT6) were digested and collected, and the concentration was adjusted to $1 \times 10^7$ cells/mL. The cells (200 μL) were injected subcutaneously into the right side of the back of 6-week-old BALB/C mice, and tumor growth was observed. When the tumor diameter reached 10 mm (13-14 days after inoculation), treatments were performed.

*Irreversible electroporation, photodynamic therapy, and irreversible electroporation + photodynamic therapy treatments:* A total of 48 female BALB/C mice with tumors were divided into 6 groups, with 8 mice in each group. The groups were as follows: control, IRE-alone 1000 V, IRE-alone 1200 V, PDT-alone, IRE+PDT-I (1000 V+PDT), and IRE+PDT-II (1200 V+PDT). The mice were anesthetized with 4% isoflurane and secured in place. For mice in the IRE-alone groups, two electrodes were inserted vertically into the tumor tissues 10 mm apart, and IRE was applied at 1000 V or 1200 V, with a pulse length of 100 μs. Ten series of pulses were used, with 100 pulses in each series and 1 s between series. For mice in the combination therapy groups, photosensitizer was injected into the tail vein, and IRE treatment (1000 or 1200 V, with other pulse parameters identical to those used in the IRE-alone groups) was administered 24 h later. After IRE, the mice were immediately illuminated with a power density of 200 mW/cm$^2$ and an illumination duration of 10 min. For mice in the PDT-alone group, photosensitizer was injected into the tail vein and illumination was performed 24 h later in a manner identical to that used for the combination therapy group. No anesthesia was used during PDT.

A Vernier caliper was used to measure tumor size, and photographs were taken once every 2 days for a total of 15 days after the above treatments. The tumor size was calculated as the long diameter × short diameter × (short diameter/2). The tumor suppression rate was calculated as the [(tumor size before operation - tumor size after operation)/tumor size before operation] × 100%.

*Ultrastructure, histopathology, and cytokine detection:* To collect tumor tissues, cancer-bearing mice were anesthetized and sacrificed by injection of an overdose of sodium pentobarbital on the first, seventh, and fourteenth days after treatment. Tumors obtained on the first day were divided vertically into two equal-sized sections, with one-half used for transmission electron microscopy (TEM) examination and the other for pathological and immunohistochemical examinations. Tissues harvested on

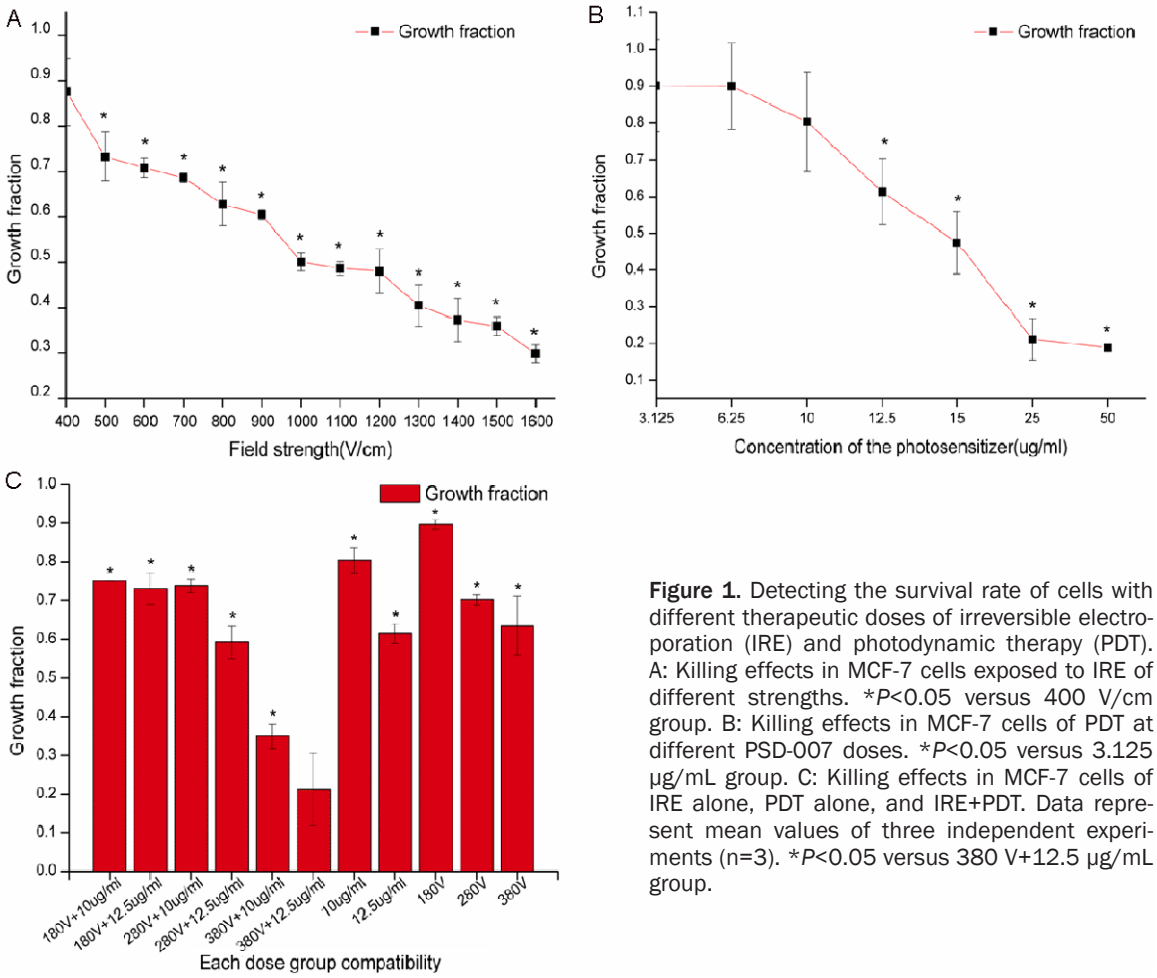


**Figure 1.** Detecting the survival rate of cells with different therapeutic doses of irreversible electroporation (IRE) and photodynamic therapy (PDT). A: Killing effects in MCF-7 cells exposed to IRE of different strengths. **P*<0.05 versus 400 V/cm group. B: Killing effects in MCF-7 cells of PDT at different PSD-007 doses. **P*<0.05 versus 3.125 μg/mL group. C: Killing effects in MCF-7 cells of IRE alone, PDT alone, and IRE+PDT. Data represent mean values of three independent experiments (n=3). **P*<0.05 versus 380 V+12.5 μg/mL group.

**Table 2.** Killing rates of irreversible electroporation combined with photodynamic therapy in MCF-7 cells

| Group | Killing rate | Q value | Combination effect |
|---|---|---|---|
| IRE-A | 19.1% | NA | NA |
| IRE-B | 29.9% | NA | NA |
| IRE-C | 36.5% | NA | NA |
| PDT-I | 19.6% | NA | NA |
| PDT-II | 38.6% | NA | NA |
| IRE-A+PDT-I | 24.9% | 0.71 | antagonism |
| IRE-A+PDT-II | 27.0% | 0.53 | antagonism |
| IRE-B+PDT-I | 26.2% | 0.60 | antagonism |
| IRE-B+PDT-II | 40.8% | 0.71 | antagonism |
| IRE-C+PDT-I | 65.1% | 1.32 | synergism |
| IRE-C+PDT-II | 78.8% | 1.29 | synergism |

Abbreviations: IRE, irreversible electroporation; NA, not applicable; PDT, photodynamic therapy.

the later 2 days were used for pathological and immunohistochemical examinations only.

For TEM, the tissues were fixed with 2.5% glutaraldehyde and then dehydrated, permeated, resin-embedded, sliced, and scanned. For pathological and immunohistochemical examinations, the tissues were fixed with 4% paraformaldehyde and then paraffin-embedded, sliced, and stained with hematoxylin and eosin or immunohistochemically stained to detect vascular endothelial growth factor (VEGF), cluster of differentiation (CD31), the nuclear-associated antigen (Ki-67), transforming growth factor (TGF-β), and tumor necrosis factor (TNF-α). Semi-quantitative analysis was performed of the immunohistochemical staining images to calculate the positive expression rate of the cytokines within five wide-field views.

*Statistical analysis*

SPSS v. 22.0 software was used for the statistical analyses, with data expressed as mean ±

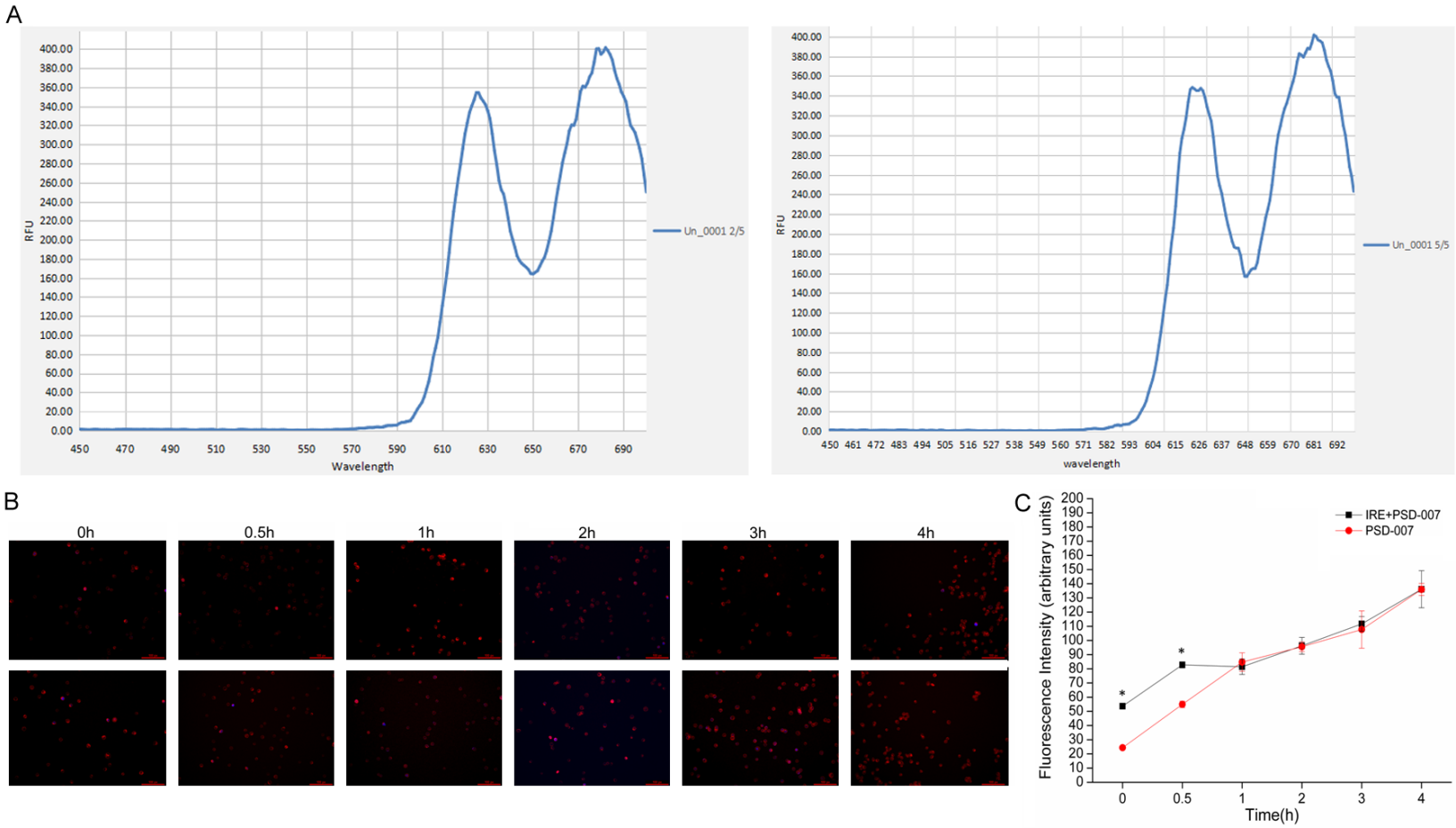


**Figure 2.** Effects of electric pulses on photosensitizer PSD-007 emission spectrum and cellular absorption. A: Emission spectrum changes before (1) and after (2) electric pulses. B: Cellular PSD-007 absorption at different times with (bottom) or without (top) irreversible electroporation (IRE). The blue signal is DNA marked by Hoechst 3342. Photosensitizer PSD-007 excited by 405-nm wavelength *laser emitted 630-nm wavelength red light, causing the cells to appear red.* C: Fluorescence intensity changes within cells over time. Data represent mean values of three independent experiments (n=3). **P*<0.05 versus PSD-007 (PSD-alone) group.

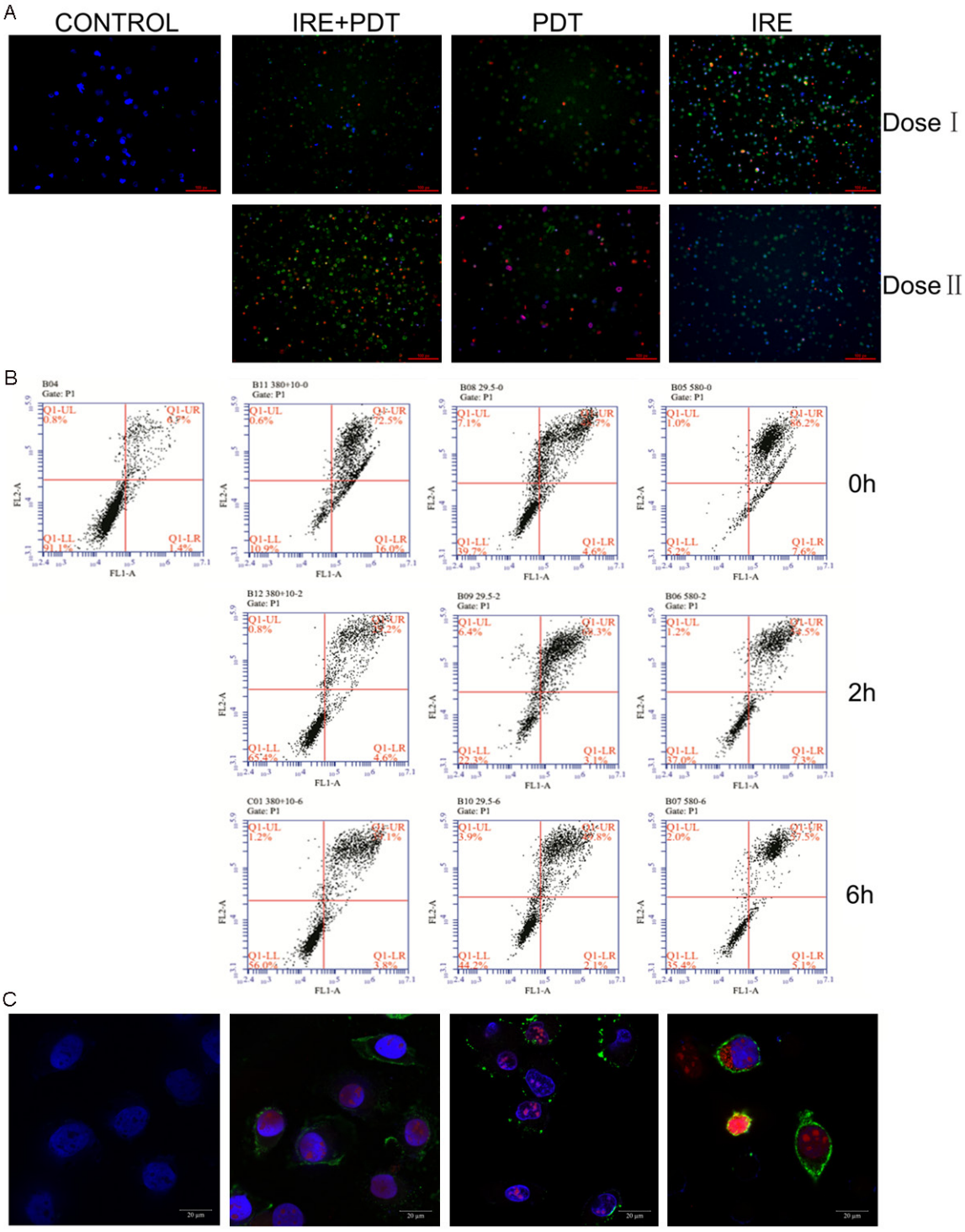


**Figure 3.** Qualitative and quantitative apoptosis detection. A: MCF-7 cells treated with irreversible electroporation (IRE), photodynamic therapy (PDT), or both (IRE+DPT) using two doses underwent detection for apoptosis by the high-content system after 24 h (10 × amplification). For IRE+PDT, dose I and II are 380 V+12.5 μg/mL and 380 V +10 μg/mL, respectively; for IRE, dose I and II are 630 V and 580 V, respectively; and for PDT, dose I and II are 32 μg/mL and 29.5 μg/mL, respectively. B: MCF-7 apoptosis, as detected by flow cytometry at 0, 2, and 6 h after treatment. C: MCF-7 apoptosis, as detected by confocal microscopy 2 h after treatment, shown at 63 × magnification. The blue signal is DNA marked by Hoechst 3342. The green signal represents eversion of phosphatidylserine in the molecular membrane marked with Annexin-FITC, which indicates early apoptosis. The red signal represents PI entry into the nuclei due to increased membrane permeability during the later stages of apoptosis. IRE, irreversible electroporation treatment alone; P DT, photodynamic therapy alone; IRE+PDT, treatment with irreversible electro-

poration and photodynamic therapy. IRE stands for the group solely treated with IRE, PDT for the group solely treated with PDT and IRE+PDT for the group treated with the combination of IRE and PDT.

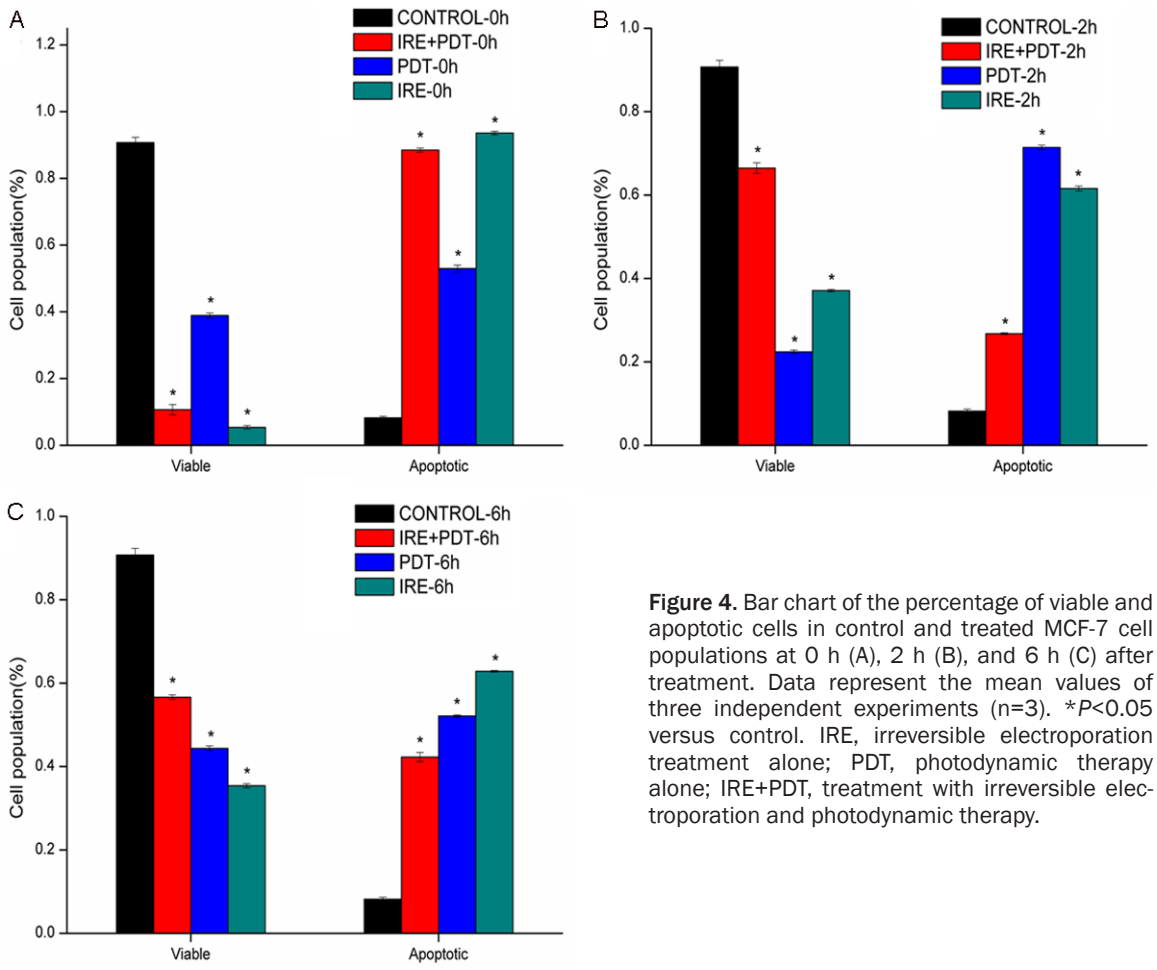


**Figure 4.** Bar chart of the percentage of viable and apoptotic cells in control and treated MCF-7 cell populations at 0 h (A), 2 h (B), and 6 h (C) after treatment. Data represent the mean values of three independent experiments (n=3). **P*<0.05 versus control. IRE, irreversible electroporation treatment alone; PDT, photodynamic therapy alone; IRE+PDT, treatment with irreversible electroporation and photodynamic therapy.

standard deviation. Differences between two groups were assessed using two-tailed Student's t-test. One-way analysis of variance was used to assess differences among more than two groups. *P*<0.05 was considered indicative of statistically significant differences.

## Results

*Cell toxicity and combination effects*

To explore the killing effects of pulsed electric fields with differing field strengths on tumor cells, cell toxicity was determined in MCF-7 cells. The results (shown in **Figure 1A**) showed that the death rate of the IRE-alone groups was positively correlated with the field strength, as more cells died with the higher field strengths. Three dose groups-IRE-A (450 V/cm), IRE-B (700 V/cm), and IRE-C (950 V/cm), which exhibited cell death rates of 20%, 30%, and 40%, respectively-were selected for subsequent combination therapy experiments.

**Figure 1B** shows the killing effects of PDT with differing doses of the photosensitizer PSD-007 in MCF-7 cells. When the concentration of photosensitizer PSD-007 was below 50 μg/mL, the killing effect of PDT on MCF-7 cells was positively correlated with the concentration of photosensitizer; that is, a higher concentration produced a higher death rate. Two dose groups-PDT-I (10 μg/mL) and PDT-II (12.5 μg/mL), which exhibited death rates of 20% and 40%, respectively-were selected for subsequent combination therapy experiments.

The killing effects of one-to-one combinations of the three IRE groups (IRE-A, IRE-B, and IRE-C) and the two PDT groups (PDT-I and PDT-II) were

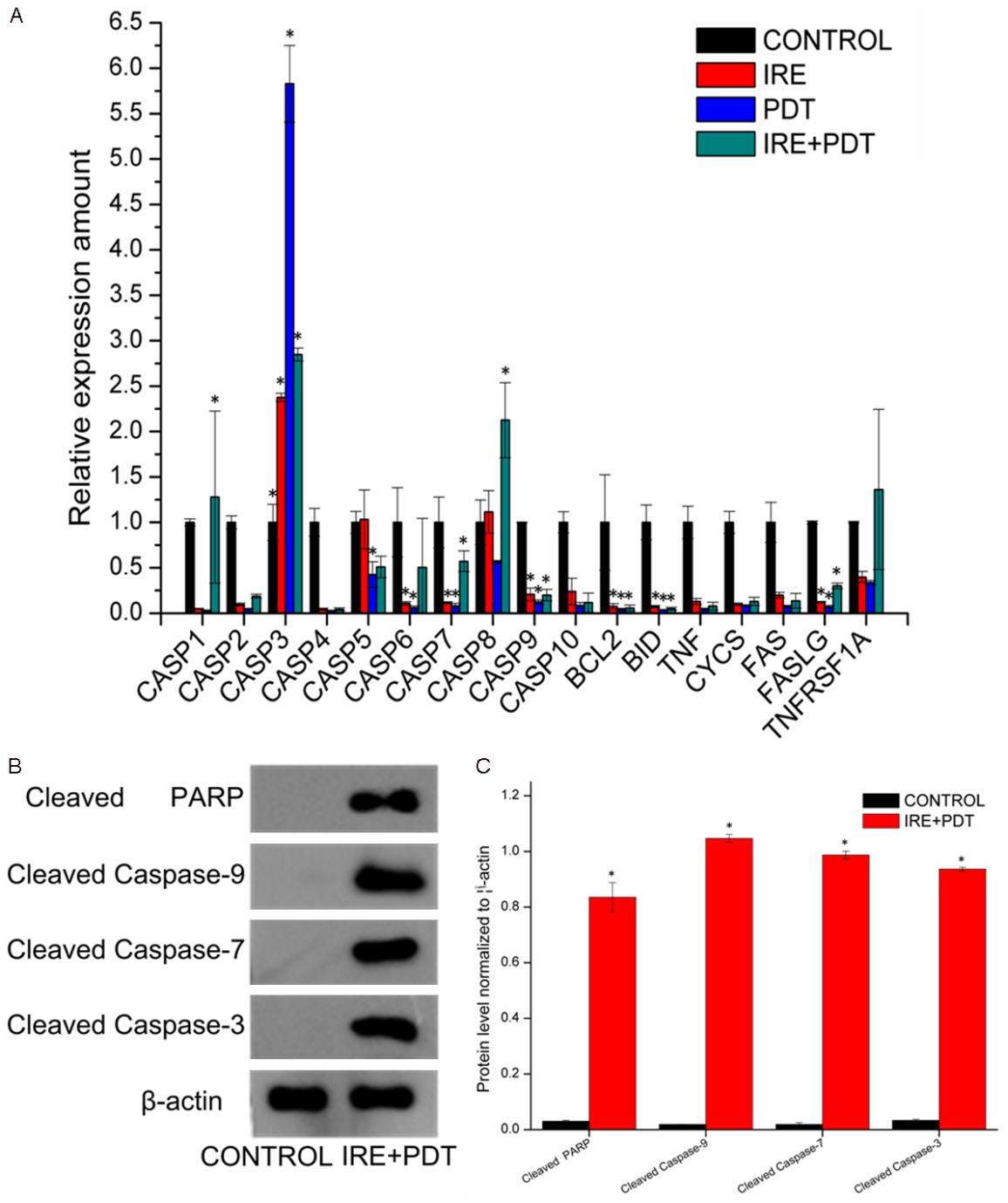


**Figure 5.** Changes in expression of apoptosis-related genes and proteins after treatment with irreversible electroporation (IRE), photodynamic therapy (PDT), and IRE+PDT. A: Apoptosis-related gene expression 2 h after MCF-7 cells were treated. B: Cleaved Caspase-3, Caspase-7, and Caspase-9 and PARP levels 6 h after MCF-7 cells were treated. C: The relative gray date from WB experiments. Data represent the mean values of three independent experiments (n=3). *$P$<0.05 versus control.

determined, as shown in **Figure 1C**. IRE-C+PDT-I and IRE-C+PDT-II were the combinations with the highest killing rates (65.1% and 78.8%, respectively). According to Jin's formula, the combination of IRE-C and PDT-I exhibited the best synergy (**Table 2**), with a q value of 1.32. Most other combinations had antagonistic effects, although the IRE-C+PDT-II combination was also synergistic. IRE-C+PDT-I was therefore used for the subsequent apoptosis detection

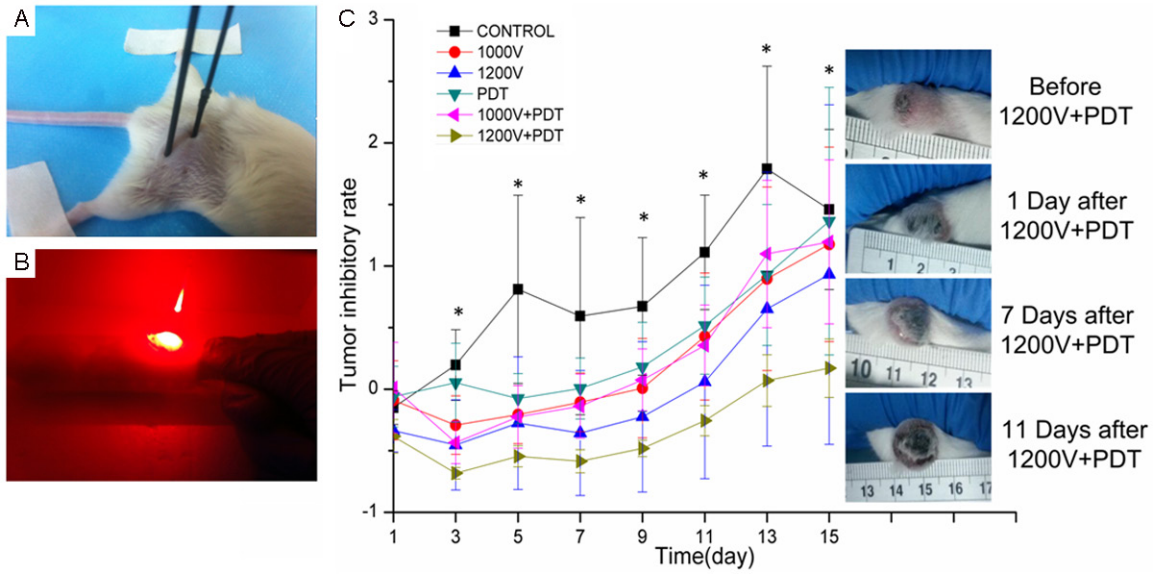


**Figure 6.** Mouse treatment procedure and tumor suppression rates after treatment. A: Irreversible electroporation (IRE) process for mice with breast cancer. B: Photodynamic therapy (PDT) process for mice with breast cancer. C: Left, changes in tumor size with treatments at different doses; right, tumors in mice treated with the combination method changed at different times. Data represent the mean values of three independent measurements (n=3). **P*<0.05 for the IRE (1200 V)+PDT (10 mg/kg) group versus control.

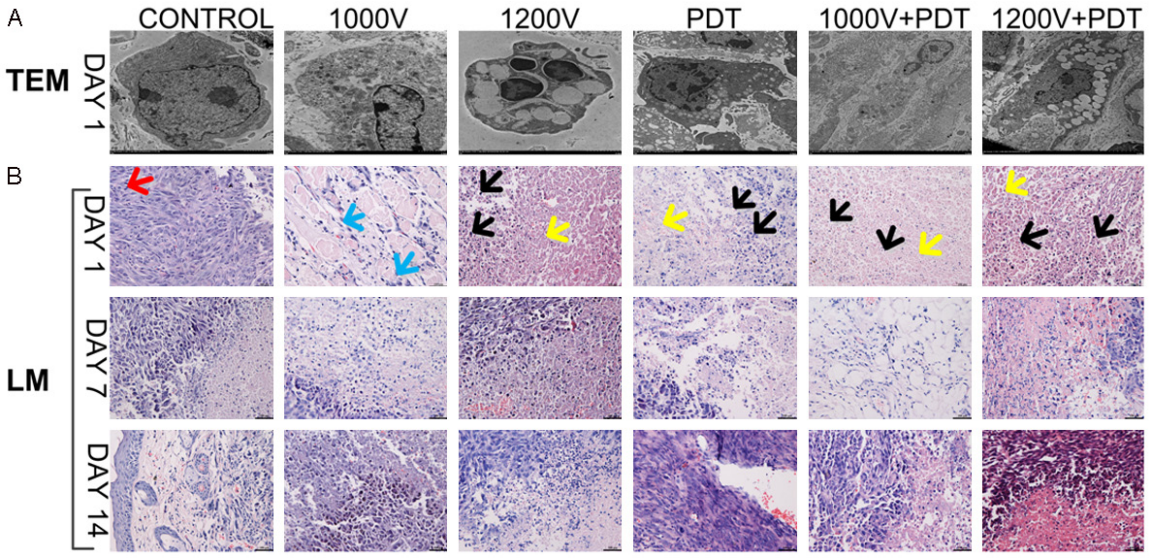


**Figure 7.** Ultrastructural and histopathological changes of various groups at different times. A: Changes in tumor tissues on the first day after treatment, as viewed under the electron microscope (TEM). B: Histopathological changes in tumor tissues at days 1, 7, and 14 after treatment, as viewed by light microscopy (LM) at 400 × magnification.

and apoptosis-related gene and protein expression studies.

*Effects of electric pulse on photosensitizer emission spectrum and absorbency*

As shown in **Figure 2A**, the photosensitizer PSD-007 appeared to have two peak values for the emission spectrum before and after the electric pulses. The peak values before the pulses occurred at 625 nm and 682 nm, and the peak values after the pulses occurred at 624 nm and 678 nm. As such differences are within the sensitivity range of the apparatus, these results indicate that the pulsed electric

fields had no obvious impact on the emission spectrum of the photosensitizer.

To explore the effects of the electric pulses on photosensitizer absorption, a high-content imaging system was used to observe cellular absorption of the photosensitizer before and after the electric fields, as shown in **Figure 2B** and **2C**. Within 30 min, the electric field improved photosensitizer absorption ($P<0.05$), but over time, the fluorescence density of the cells in the group without an electric field stimulation increased. After 4 h, cells in all groups exhibited a similar fluorescence density.

*Apoptosis detection*

Apoptosis was detected qualitatively, quantitatively, and at the cell morphology level with a high-content imaging system, flow cytometry, and confocal laser scanning microscopy, respectively. **Figure 3A** shows apoptosis with the high-content cell imaging and analysis system in the three groups of cells 24 h after treatment. Apoptosis was observed in all three groups. The IRE (380 V)+ PDT (10 μg/mL) combination group had the highest apoptosis rate and exhibited the typical characteristics of early apoptosis, such as phosphatidylserine molecular membrane eversion (green fluorescent signal), and late apoptosis, such as karyopyknosis (red fluorescent signal).

The three groups with the strongest apoptosis results-IRE-II, PDT-II, and IRE+PDT-II-were selected by high-content imaging analysis and underwent qualitative analysis by flow cytometry. The results are shown in **Figures 3B**, **4**. Apoptosis occurred in all groups to various degrees. At 0 h (immediately after treatment), the apoptosis rates of the IRE+PDT-II, PDT-II, and IRE-II groups were 16.0%, 4.6%, and 7.6%, respectively; the rate of the combination group was significantly higher than that of the other two groups. At 6 h, the apoptosis rates decreased, while the necrosis rates increased.

Apoptosis detected by laser scanning confocal microscopy is shown in **Figure 3C**. The combination therapy group exhibited clear apoptotic features, including phosphatidylserine molecular membrane eversion, increased membrane permeability, nuclear crenation, karyorrhexis in some cells, and other apoptotic morphologies.

*Expression of apoptosis-related genes and proteins*

When evaluating the presence of 17 genes related to apoptosis, we found that expression of cysteine-aspartic acid protease (Caspase) family and death receptor-related genes in the various treatment groups changed as early as 2 h post-treatment (**Figure 5A**). Expression of Caspase-3 was higher in all treatment groups than in the control group ($P<0.05$), and expression in the PDT-alone group was the greatest: 2.5 times that of the IRE-alone group and 2 times that of the combination therapy group. Caspase-9, Bc12, and Bid expression decreased in all three treatment groups compared with control at 2 h post-treatment ($P<0.05$). The combination therapy group had the highest Caspase-8 expression, which was 1.9 times that of the PDT-alone group and 3.8 times that of the IRE-alone group. Among all of the treatment groups, expression of Caspase-6 and Caspase-7 was highest in the combination therapy group, but expression of both was lower than in the control. Expression of Caspase-5 was highest in the IRE-alone group, but it was lower in the PDT-alone and combination therapy groups than in controls ($P<0.05$). Expression of FASLG and TNFRSF1A in the combination therapy group was higher than in the IRE-alone and PDT-alone groups, but FASLG expression was lower than in the control group.

To cleaved Caspase-7 and cleaved Caspase-3 fragments, allowing Caspase-3 to activate poly (ADP-ribose) polymerase (PARP), initiating apoptosis. We performed western blotting to analyze the expression of Caspase-3, Caspase-7, and Caspase-9 fragments and PARP. As shown in **Figure 5B** and **5C**, expression of all of these proteins was significantly higher in the combination therapy group than in the control group ($P<0.05$).

*Tumor suppression rate*

Tumor sizes in mice from all treatment groups became smaller, as tumor growth was suppressed after treatment (**Figure 6**). On day 1 post-treatment, tumor suppression rates of the groups were 9.0% for IRE-alone (1000 V), 33.7% for IRE-alone (1200 V), 6.1% for PDT-alone, 1.2% for IRE (1000 V)+PDT (10 mg/kg), 38.3% for IRE (1200 V)+PDT (10 mg/kg). On day 3

post-treatment, the tumor suppression rates of the five treatment groups reached peak values: 29.1%, 45.3%, 5.3%, 43.4%, and 68.3%, respectively. These results indicate that the combination therapy groups produced more tumor suppression than the IRE-alone and PDT-alone groups, with the IRE (1200 V)+PDT (10 mg/kg) producing the most suppression ($P<0.05$).

*Histopathological and ultrastructure observation*

**Figure 7A** shows TEM images of tumors from the various groups on the first day after treatment. Varying degrees of apoptosis occurred in all treatment groups, as evidenced by heavy condensation and chromatin marginalization, and nuclear fragmentation during late apoptosis. In particular, many typical apoptotic bodies appeared in the combination therapy group, which was the most obvious sign of apoptosis.

The results of histopathological analysis showed that cells in the control group had large nuclei, with clearly visualized cytoplasts and nucleoli, as well as abundant cytoplasm. The tumors were nest-shaped with typical signs of karyokinesis (red arrow in **Figure 7B**) and were infiltrated with only a few inflammatory cells. As the tumors grew, the cells began to necrose because of the limited blood supply. In all treatment groups, signs of necrosis, such as nucleus fragmentation (black arrows in **Figure 7B**) and indistinct cytoplast boundaries (blue arrows in **Figure 7B**), were apparent the first day after treatment. Tumors from the combination therapy groups exhibited necrosis of large tumor cells because of the limited blood supply, obvious infiltration by inflammatory cells, and prominent fibrous tissue (yellow arrows in **Figure 7B**). On the seventh day after treatment, invasive growth of tumor cells was found at the edge of necrotic tissue in the IRE+PDT groups. On the fourteenth day after treatment, two trends were found within tumor tissue: coagulative necrosis of tumor cells in large areas and massive recurrence and proliferation of residual tumor cells.

*Immunostaining*

We detected VEGF, CD31, Ki-67, TGF-β, and TNF-α expression in tumor tissues. On the first day after treatment, angionecrosis occurred in the combination therapy groups, with positive VEGF and CD31 staining decreased to 24.4% in the IRE (1200 V)+PDT (10 mg/kg) group, as shown in **Figure 8A** and **8B**. On the seventh day after treatment, new vessels were found in the IRE (1200 V)+PDT (10 mg/kg) group, with positive VEGF and CD31 staining increased to 28.6%. TGF-β was actively expressed in the control group on all days, and the rate of positive TGF-β staining was lower in all treatment groups than in control at all times, except in the PDT-alone group on first day after treatment. On the seventh day after treatment, the percentage of positive TGF-β staining in the IRE (1200 V)+PDT (10 mg/kg) group began to increase, and on the fourteenth day after treatment, it reached 22.2%. In the control group, the rate of positive Ki-67 staining was 27.5% and the rate of positive TNF-α staining was only 19.4% on the first day after treatment. On the first day after treatment, Ki-67 was decreased in all treatment groups, and TNF-α was increased in most treatment groups. On the seventh day after treatment, the percentage of positive Ki-67 staining in the treatment groups increased, and positive staining for TNF-α decreased for most treatment groups. On the fourteenth day after treatment, the percentage of positive Ki-67 staining continued to increase, whereas staining of TNF-α continued to decrease in the treatment groups. The percentage of positive TNF-α cells was significantly lower in the IRE (1200 V)+PDT (10 mg/kg) than in the control group on the fourteenth day ($P<0.05$).

## Discussion

At the cellular level, we used cytotoxicity testing of breast cancer cell lines to screen various combinations of low-dose IRE and PDT: IRE-A (450 V/cm), IRE-B (700 V/cm), IRE-C (950 V/cm), PDT (PDT-I, 10 μg/mL and PDT-II, 12.5 μg/mL), Using Jin's formula, we determine that the best combination was IRE-C+PDT-I, which demonstrated synergistic cytotoxic effects that were much higher than those produced by IRE or PDT alone. The rate of killing MCF-7 cells with combination therapy was 1.78 times with IRE alone and 3.32 times than with PDT alone. The tumor suppression rate was 68.3% in the IRE (1200 V)+PDT (10 mg/kg) treatment group by the third day after treatment, which was 1.5 times of the IRE-alone (1200 V) group. Com-

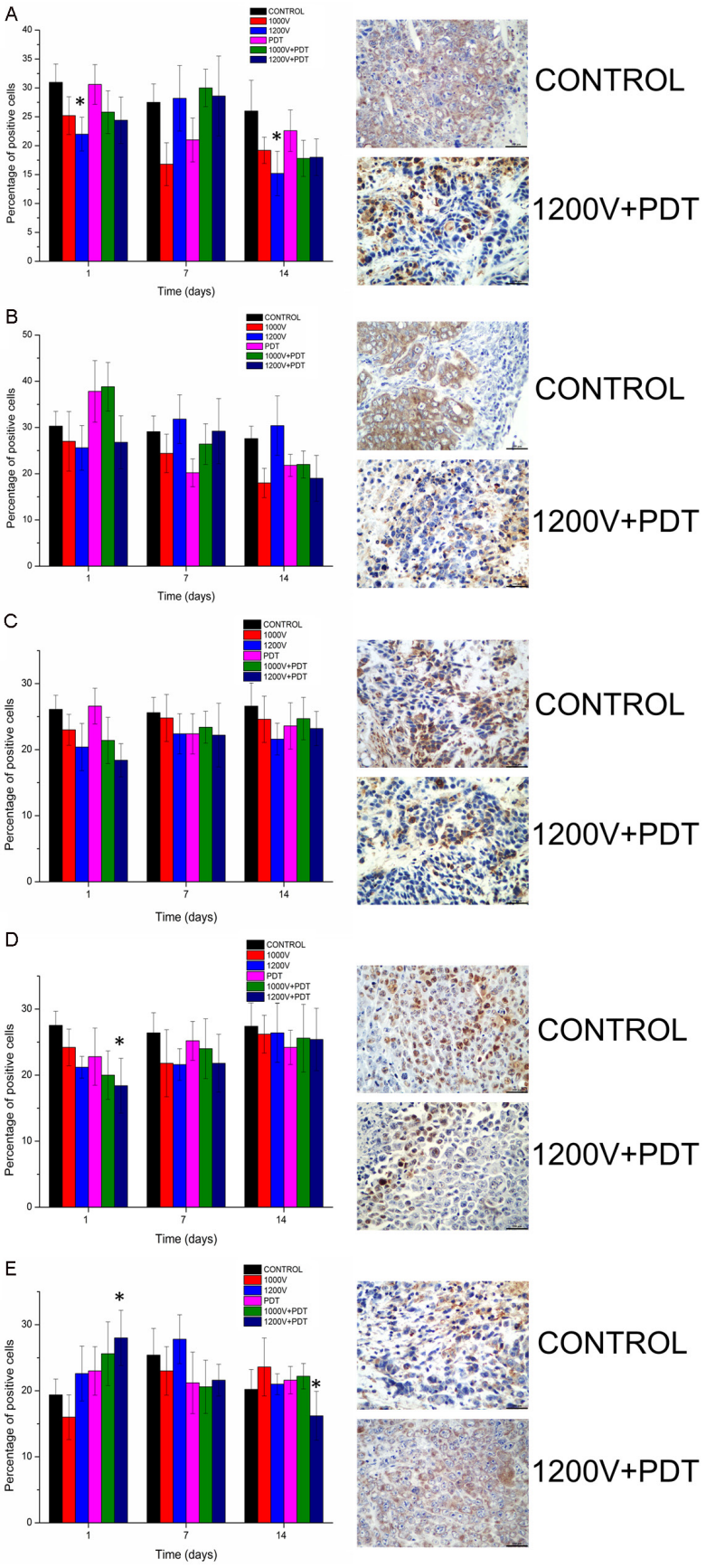


**Figure 8.** Changes in percentages of positively-stained cells for tumor-related factors in the various irreversible electroporation (1000V and 1200V), photodynamic therapy (PDT), and IRE+PDT (1000V+PDT and 1200V+PDT) groups, as determined by immunohistochemical staining. A: Left, VEGF expression; right, tissue changes in the control and 1200V+PDT groups. B: Left, CD31 expression; right, tissue changes in the control and 1200V+PDT groups. C: Left, TGF-β expression; right, tissue changes in the control and 1200V+PDT groups. D: Left, Ki-67 expression; right, tissue changes in the control and 1200V+PDT groups. E: Left, TNF-α expression; right, tissue changes in the control and 1200V+PDT groups. Light microscopy images are shown at 400x magnification. Data represent the mean values from three independent measurements (n=3). **P*<0.05 versus control.

bination therapy substantially improved anti-tumor effects of IRE and PDT, suggesting that it may have considerable potential as a therapeutic option for breast cancer.

In experiments examining the killing efficiency of IRE and electro-chemotherapy in malignant glioma, Neal et al. [24] reported that the combination increased killing effects by 2 to 3 times, compared with IRE alone. However, this may not be the ideal approach because chemotherapy drugs have poor targeting and substantial side effects. In the current study, we used PDT instead, as it is safe, without significant side effects, and can be used for repeated treatments. In addition, more conventional minimally invasive ablation causes coagu-

lative necrosis and adverse effects, but combined IRE and PDT induces cell apoptosis, which can reduce the body's inflammatory response and restore the integrity of normal body tissues.

Apoptosis plays a key role in cancer treatment, and the IRE ablation used in this study has been previously demonstrated to produce apoptosis [7, 25, 26] and necrosis of tumor cells. Apoptosis is also an important tumor-killing mechanism for PDT [27, 28]. In the current study, we have demonstrated that apoptosis is important for the killing of tumor cells by IRE+PDT combination therapy. Our cell experiment results showed that apoptosis occurred in all three treatment groups, but flow cytometry results indicated that the apoptosis rate of MCF-7 cells treated with combination therapy was 3.5 times and 2.1 times higher than the rates of cells treated with PDT alone and IRE alone, respectively. Our *in vivo* experiments also showed that apoptosis in murine breast tumors was substantially greater in tumors treated with combination therapy than in those treated with IRE or PDT alone. In their study of histological changes at different time points after IRE ablation of tumor tissue, Kim et al. [8] demonstrated that apoptosis rates reached peak values at 24 h after treatment, a finding that is consistent with our current results.

There are many inductive pathways for cell apoptosis [29]. One is the cell surface receptor-mediated pathway, in which factors induce apoptosis through apoptosis-related receptors on the surface of cell membranes. These receptors mainly belong to tumor necrosis factor receptor (TNFR) family, such as TNFR and FAS, but they also include the TNF-related apoptosis-inducing ligand receptor (TRAIL-R). The other pathway is the mitochondrial-mediated pathway, which is a rapid apoptosis pathway, as all factors for apoptosis are available and only require activation. By screening 17 apoptosis-related genes in this study, we found that IRE+PDT combination therapy activated many apoptosis pathways. As shown in **Figure 9**, increased expression of apoptosis-related genes occurred in all three treatment groups. In the IRE-alone and PDT-alone groups, apoptosis occurred mainly through the mitochondrial-mediated pathway, whereas strong expression of genes involved in both the apoptosis-related receptor and mitochondrial-mediated pathways was observed in the combination therapy group, which may explain why the highest apoptosis rate occurred in this group.

It is also noteworthy that Caspase-1 expression in the combination therapy group was much higher than that observed in the IRE-alone and PDT-alone groups. Caspase-1 plays an important role in regulating inflammatory reactions and apoptosis. It has been found that excessive Caspase-1 expression can activate Caspase-3 and Caspase-9 [30], eventually causing apoptosis. Therefore, increased Caspase-1 expression in the combination therapy group suggests that Caspase-1 may promote apoptosis and participate in the inflammatory reaction within cells, releasing cellular contents to activate immune reactions. By contrast, Caspase-1 expression changed little in the IRE-alone and PDT-alone groups, supporting the view that combination therapy more effectively activates immune reactions, inducing the body to suppress tumors and instilling long-lasting treatment benefits.

TNF-α expression relates to the health of tumor cells, whereas Ki-67 expression relates to the growth and invasion of tumors, and TGF-β expression relates to the degree of tumor invasion. Changes in TNF-α, Ki-67, and TGF-β expression after combination therapy verified the presence of direct killing of tumor cells. We also found that blood vessel injury appeared to be one of the anti-tumor mechanisms of combination therapy, as VEGF and CD31 did not recover to normal levels until 2 weeks after treatment. Nuccitelli et al. [31] reported results that were consistent with ours. Using ultrasonic Doppler scanning, they found that blood flow ceased within 15 min after the end of pulsed electric field therapy in a mouse melanoma model, and histological examination demonstrated that blood flow did not return to normal for approximately 2 weeks, the exact time of which correlated with the level of tumor damage.

## Conclusions

Using both *in vivo* and *in vitro* methods, we showed that IRE+PDT combination therapy produced superior tumor killing than IRE or PDT alone, and that apoptosis plays a key role in the

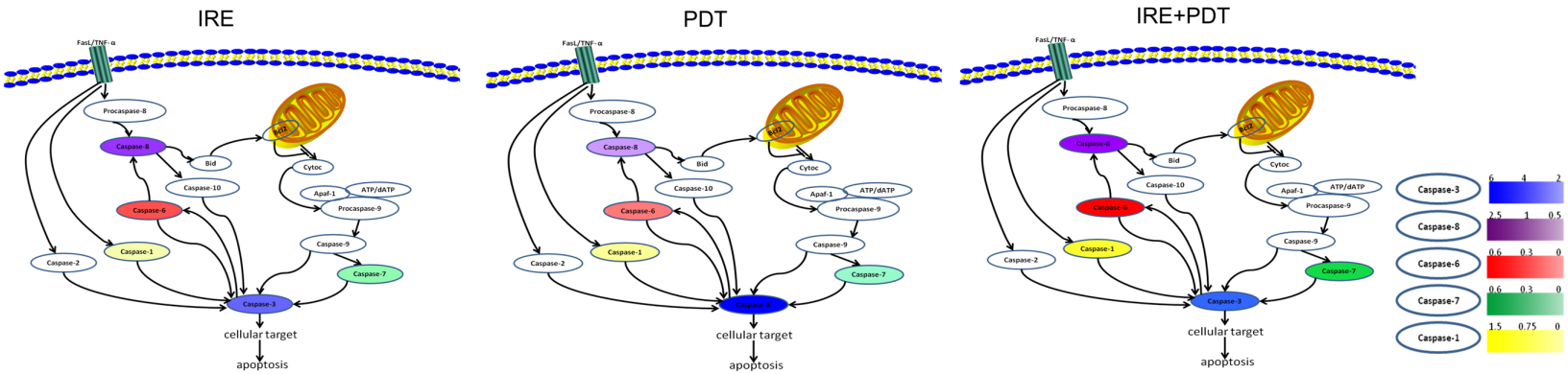


**Figure 9.** Expression pathways of apoptosis-related genes in the different treatment groups. IRE, irreversible electroporation treatment alone; PDT, photodynamic therapy alone; IRE+PDT, treatment with irreversible electroporation and photodynamic therapy.

anti-tumor mechanisms of combination therapy. IRE+PDT combination therapy, therefore, appears to be a promising treatment for solid tumors in humans. We propose that the combination of IRE and PDT will provide a new therapeutic regimen that overcomes incomplete tumor boundary ablation that often occurs with IRE alone. In future experiments, we will focus on optimizing the dosage of combination therapy and generating a complete and accurate mechanistic explanation for the effects of this therapy.

## Acknowledgements

This study is supported by the Key Technologies Research and Development Program of Tianjin (14ZCDZSY00037).

## Disclosure of conflict of interest

None.

**Address correspondence to:** Zhixiao Xue, Biomedical Engineering and Technology College, Tianjin Medical University, Tianjin 300070, China. Tel: 13821074-823; E-mail: xuezhixiao@126.com; Huijuan Yin, Lab of Laser Medicine, Institute of Medical Engineering, Chinese Academy of Medical Sciences and Peking Union Medical College, Tianjin 300192, China. Tel: 13662176304; E-mail: yinzi490@163.com

## References

[1] Jemal A, Bray F, Center MM, Ferlay J, Ward E and Forman D. CA: a cancer journal for clinicians. CA Cancer J Clin 2011; 61: 69-90.

[2] Davalos RV, Mir LM and Rubinsky B. Tissue ablation with irreversible electroporation. Ann Biomed Eng 2005; 33: 223-231.

[3] Edd JF, Horowitz L, Davalos RV, Mir LM and Rubinsky B . In vivo results of a new focal tissue ablation technique irreversible electroporation. IEEE Trans Biomed Eng 2006; 53: 1409-1415.

[4] Bower M, Sherwood L, Li Y and Martin R. Irreversible electroporation of the pancreas: definitive local therapy without systemic effects. J Surg Oncol 2011; 104: 22-28.

[5] Lee EW, Wong D, Prikhodko SV, Pere A, Tran C, Lonh CT and Kee ST. Electron microscopic demonstration and evaluation of irreversible electroporation-induced nanopores on hepatocyte membranes. J Vasc Interv Radiol 2012; 23: 107-113.

[6] Guo Y, Zhang Y, Klein R, Nijm GM, Sahakian AV, Omary RA , Yang GY and Larson AC. Irreversible electroporation therapy in the liver: longitudinal efficacy studies in a rat model of hepatocellular carcinoma. Cancer res 2010; 70: 1555-1563.

[7] Kim HB, Sung CK, Baik KY, Moon KW, Kim HS, Yi JH, Jung JH, Moon MH and Choi OK. Changes of apoptosis in tumor tissues with time after irreversible electroporation. Biochem Biophys Res Commun 2013; 435: 651-656.

[8] Lencioni R , Crocetti R. Local-regional treatment of hepatocellular carcinoma. Radiology 2012; 262: 43-58.

[9] Niessen C, Beyer LP, Pregler B, Dollinger M, Trabold B, Schlitt HJ, Jung EM, Stroszczynski C and Wiggermann P. Percutaneous ablation of hepatic tumors using irreversible electroporation: a prospective safety and midterm efficacy study in 34 patients. J Vasc Interv Radiol 2016; 27: 480-486.

[10] Bagla S, Papadouris D. Percutaneous irreversible electroporation of surgically unresectable pancreatic cancer: a case report. J Vasc Interv Radiol 2012; 23: 142-145.

[11] Månsson C, Bergenfeldt M, Brahmstaedt R, Karlson BM, Nygren P and Nilsson A. Safety and preliminary efficacy of ultrasound-guided percutaneous irreversible electroporation for treatment of localized pancreatic cancer. Anticancer Res 2014; 34: 289-293.

[12] Pech M, Janitzky A, Wendler JJ, Strang C, Blaschke S, Dudeck O, Riche J and Liehr UB. Irreversible electroporation of renal cell carcinoma: a first-in-man phase i clinical study. Cardiovasc Intervent Radiol 2011; 34: 132-138.

[13] Thomson KR, Cheung W, Ellis SJ, Federman D, Kavnoudias H, Loader-Oliver D, Roberts S, Evans P, Ball C and Haydon A. Investigation of the safety of irreversible electroporation in humans. J Vasc Interv Radiol 2011; 22: 611-621.

[14] Deodhar A, Dickfeld T, Single GW, Hamilton RH, Sofocleous CT, Maybody M, Gónen M, Rubinsky B and Solomon SB. Irreversible electroporation near the heart: ventricular arrhythmias can be prevented with ECG synchronization. AJR Am J Roentgenol 2011; 196: W330-W335.

[15] Usman M, Moore W, Talati R, Watkins K and Bilfinger TV. Irreversible electroporation of lung neoplasm: a case series. Med Sci Monit 2012; 18: CS43-CS7.

[16] Gary Onik, Rubinsky B. Irreversible electroporation: first patient experience focal therapy of prostate cancer. Irreversible Electroporation 2010: 235-247.

[17] Rubinsky B. Irreversible electroporation in medicine. Technol Cancer Res Treat 2007; 6: 255-259.

[18] Davalos RV, Rubinsky B. Temperature considerations during irreversible electroporation. Int J Heat Mass Transf 2008; 51: 5617-5622.

[19] Al-Sakere B, André F, Bernat C, Connault E, Opolon P, Davalos RV, Rubinsky B and Mir LM. Tumor ablation with irreversible electroporation. PLoS One 2007; 2: e1135.
[20] Neal II RE, Davalos RV. The feasibility of irreversible electroporation for the treatment of breast cancer and other heterogeneous systems. Ann Biomed Eng 2009; 37: 2615-2625.
[21] Ivorra A, Rubinsky B. In vivo electrical impedance measurements during and after electroporation of rat liver. Bioelectrochemistry 2007; 70: 287-295.
[22] Daniels C, Rubinsky B. Electrical field and temperature model of nonthermal irreversible electroporation in heterogeneous tissues. J Biomech Eng 2009; 131: 071006-1-071006-12.
[23] Wendler JJ, Ricke J, Pech M, Fischbach F, Jűrgens J, Siedentopf S, Roessner A, Porsch M, Baumunk D, Schostak M, Kőllermann J and Liehr UB. First delayed resection findings after irreversible electroporation of human localised renal cell carcinoma in the irene pilot phase 2a trial. Cardiovasc Intervent Radiol 2016; 39: 239-250.
[24] Neal RE 2nd, Rossmeisl JH Jr, D'Alfonso V, Robertson JL, Garcia PA, Elankumaran S and Davalos RV. In vitro and numerical support for combinatorial irreversible electroporation and electrochemotherapy glioma treatment. Ann Biomed Eng 2014; 42: 475-487.
[25] Zhang Z, Li W, Procissi D, Tyler P, Omary RA and Larson AC. Rapid dramatic alterations to the tumor microstructure in pancreatic cancer following irreversible electroporation ablation. Nanomedicine 2014; 9: 1181-1192.
[26] Long G, Bakos G, Shires PK, Gritter L, Crissman JW, Harris JL and Clymer JW. Histological and finite element analysis of cell death due to irreversible electroporation. Technol Cancer Res Treat 2014; 13: 561-569.
[27] Plaetzer K, Kiesslich T, Oberdanner CB and Krammer B. Apoptosis following photodynamic tumor therapy: induction, mechanisms and detection. Curr Pharm Des 2005; 11: 1151-1165.
[28] Kubiak M, Łysenko L, Gerber H and Nowak R. Cell reactions and immune responses to photodynamic therapy in oncology. Postepy Hig Med Dosw 2016; 70: 735-742.
[29] Duprez L, Wirawan E, Berghe VT and Vandenabeele P. Major cell death pathways at a glance. Microbes Infect 2009; 11: 1050-1062.
[30] Syed FM, Hahn HS, Odley A, Guo Y, Vallejo JG, Lynch RA, Mann DL, Bolli R and Dorn II GW . Proapoptotic effects of caspase-1/interleukin-converting enzyme dominate in myocardial ischemia. Circ Res 2005; 96: 1103-1109.
[31] Nuccitelli R, Pliquett U, Chen XH, Ford W, Swanson RJ, Beebe SJ, Kolb JF and Schoenbach KH. Nanosecond pulsed electric fields cause melanomas to selfdestruct. Biochem Biophys Res Commun 2006; 343: 351-360.